Author(s): Manninen, A. J. & Pekola, Jukka & Kira, G. M. & Ruutu, J. P. & Babkin, A. V. & Alles, H. & Lounasmaa, O. V.

Title: First optical observations of superfluid He 3

Year: 1992

Version: Final published version

Please cite the original version:

Manninen, A. J. & Pekola, Jukka & Kira, G. M. & Ruutu, J. P. & Babkin, A. V. & Alles, H. & Lounasmaa, O. V. 1992. First optical observations of superfluid He 3. Physical Review Letters. Volume 69, Issue 16. P. 2392-2395. ISSN 0031-9007 (printed). DOI: 10.1103/physrevlett.69.2392.

First Optical Observations of Superfluid ^{3}He

A. J. Manninen, J. P. Pekola,[a] G. M. Kira, J. P. Ruutu, A. V. Babkin, H. Alles, and O. V. Lounasmaa

Low Temperature Laboratory, Helsinki University of Technology, 02150 Espoo, Finland

(Received 7 August 1992)

The shape of the free surface of rotating superfluid ^{3}He-*B* has been investigated optically. The drastic change in viscosity at the superfluid transition was *seen* directly. Focusing of light reflected from the liquid surface and expansion of the light beam when it travels through the ^{3}He sample show that the meniscus of the rotating superfluid has the same parabolic shape as that of the normal liquid, which implies an equilibrium density of vortices. The fountain effect in ^{3}He-*B* could be seen directly as well: Liquid accumulates into the illuminated region.

PACS numbers: 67.50.Fi

The existence of vortices in superfluid ^{4}He was first concluded on the basis of optical measurements [1]. The meniscus $z(r)$ of a superfluid sample that was rotated with angular velocity Ω was of the form

$$z(r)=\Omega^2 r^2/2g\,, \tag{1}$$

like in an ordinary liquid, which implied that the superfluid component was moving with the cylindrical container. The classical surface profile was confirmed later by interferometry [2].

Rotation of the superfluid component seemed, at first, to be in conflict with the irrotational nature ($\nabla\times\mathbf{v}_s=0$) of its velocity field $\mathbf{v}_s$, which means that in a simply connected rotating cylinder the superfluid component should stay at rest. Feynman [3] suggested that a lattice of singular vortex lines forms in a rotating vessel: Around each vortex the superfluid component has a velocity field of the form $1/r$, for which $\nabla\times\mathbf{v}_s=0$. A direct experimental proof of vortices was obtained by Williams and Packard [4], who were able to see them in superfluid ^{4}He by detecting negative ions trapped by the vortex cores.

In this Letter we report the first optical experiments on superfluid ^{3}He. We have investigated the shape of the free surface of the rotating liquid down to $T\simeq 0.7$ mK; the minimum reported temperature for earlier optical experiments is well above 10 mK due to thermal radiation through observation windows [5]. The scheme of our experimental setup is shown in Fig. 1. Instead of windows, optical fibers are used to communicate between the low-temperature parts of the cryostat and the video camera at room temperature. All effects that we report on can be seen in a video film that we have produced.

Referring to Fig. 1, the source of illumination LA is a 5-mW He-Ne laser which rotates with the cryostat. Light enters into the cold parts of the apparatus through a single-mode optical fiber F; it is first collimated by the convex lens L3 to a parallel beam of 2 mm diameter. Light is then conducted into the sample cell OC via a beam splitter BS and two mirrors, M1 and M2; the diameter of the beam is expanded to 10 mm by two plano-convex fused silica lenses L1 and L2, 300 mm apart and with focal lengths $f_1=50$ mm and $f_2=250$ mm, respectively. Light reflected from the bottom window WW of OC or from the surface of the ^{3}He sample S is guided through L2, L1, and BS into the lower end of FB, a 2.2-mm-diam coherent bundle of 30000 optical fibers. At room temperature light is monitored by a video camera CCD, focused to the upper end of FB by a positive lens L4. Unreflected light through the sample cell is guided onto a black surface on the radiation shield ST by a 45° mirror M3; ST is thermally anchored to the still and M3 to the mixing chamber MXC of the dilution refrigerator.

The top TW and bottom WW windows of OC were made of fused silica. TW is tilted and WW wedged by 2°, so that reflection from the reference plane, i.e., the upper surface of WW, only reaches the camera. This plane was antireflection coated to increase the contrast of optical interference. The inner diameter of OC is as large as 20 mm to diminish the capillary rise of ^{3}He on the cylindrical side wall. The sample S in the optical cell

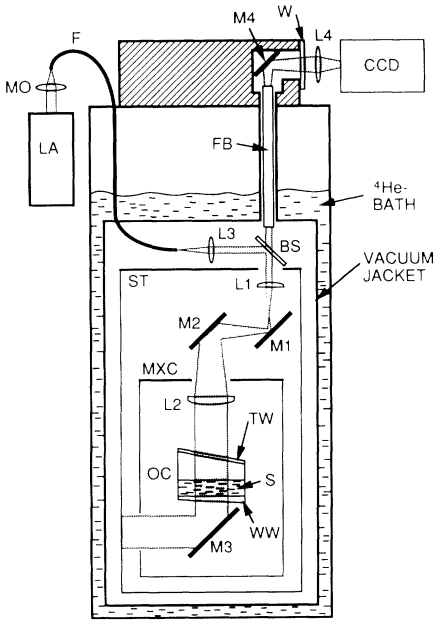

FIG. 1. Schematic illustration of the experimental setup (not to scale). Explanation of symbols: MO, microscope objective; M1, . . . , M4, aluminum coated mirrors; W, window. For other abbreviations, see text.

was connected to the heat exchanger volume of the nuclear cooling stage through a 1-mm hole (not shown in Fig. 1) in the side wall of OC, just above the bottom window. The sample was typically illuminated by 50-ms pulses every 2 s. The temperature was measured by a pulsed platinum NMR thermometer. All our experiments were made in zero magnetic field and, naturally, at $P=0$.

Our first observations of the dramatic change in the viscosity of the liquid around the superfluid transition point T_c demonstrated that we really were able to *see* superfluid ^{3}He. With about a 1-mm layer of the liquid in OC and with the rotation axis of the cryostat slightly tilted with respect to gravity, the light beam refracted by the liquid surface and reflected from WW was monitored. The intensity of the received light was not spatially uniform but had some inhomogeneities caused by aberrations in the optical components and, sometimes, by droplets of ^{3}He condensed under TW. These "markers" enabled us to follow the lateral motion of the reflected beam.

In the superfluid state, the viscosity of ^{3}He is so low that the free surface remained perpendicular to gravity while the cryostat was rotated slowly, about 0.1 rad/s. This means that in the coordinate system of the CCD camera, which rotated with the slightly tilted cryostat, the liquid surface and, consequently, the light beam that was refracted by it were precessing. When the sample was warmed up to the normal state while still rotating, precession suddenly stopped at T_c: Normal liquid, which is very viscous at low temperatures, was forced to follow the walls of OC. When the liquid was warmed further, its viscosity became finally so low that precession resumed.

The free meniscus $z(r)$ [see Eq. (1)] of a classical liquid or of a superfluid with an equilibrium number of vortices acts as a parabolic mirror with a focal length $f=g/2\Omega^2$. In a vortex-free state, in which the superfluid component ρ_s/ρ stays at rest and only the normal fraction ρ_n/ρ rotates with the container [6], the surface profile is

$$z(r)=(\rho_n/\rho)\Omega^2 r^2/2g \qquad (2)$$

and $f=(\rho/\rho_n)g/2\Omega^2$. At a certain Ω, the focal point of the optical system produced by the meniscus of the liquid and the lenses L_1 and L_2 is in the plane of the lower end of FB (see Fig. 1): Light reflected from the liquid surface thus focuses into a single point on the CCD sensor. Using the dimensions and other properties of our apparatus we expect this to take place at $\Omega_{foc}=2.1\pm0.1$ rad/s, if the meniscus has the classical form of Eq. (1). In a vortex-free state, Ω_{foc} of the superfluid would be enhanced, according to Eq. (2), by the factor $(\rho/\rho_n)^{1/2}$.

The observation of focusing is shown in Fig. 2, where interference patterns between light reflected from the surface of the superfluid and from the bottom window of the sample cell are presented at several rotation velocities.

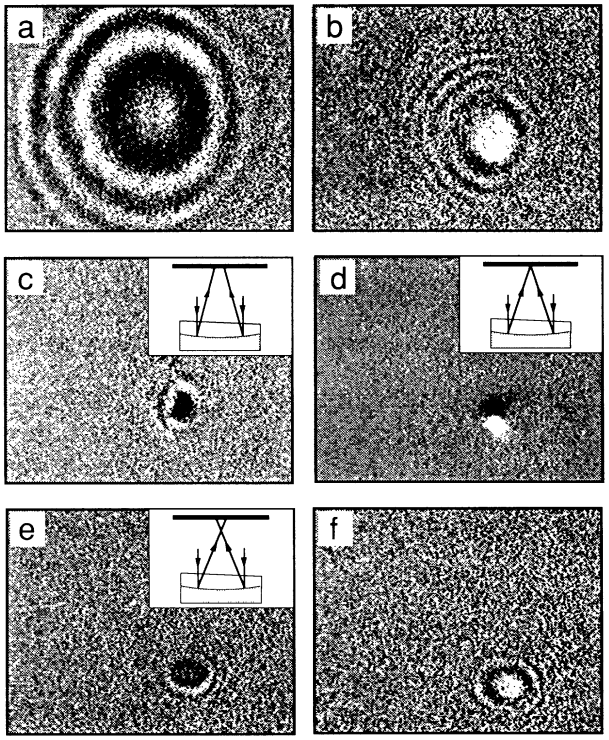

FIG. 2. Interference patterns produced by light reflected from the bottom window WW of the sample cell OC (see Fig. 1) and from the superfluid surface at $T/T_c\simeq0.75$. (a) $\Omega=0$, (b) $\Omega=1.6$ rad/s, (c) $\Omega=2.0$ rad/s, (d) $\Omega=2.25$ rad/s, (e) $\Omega=2.5$ rad/s, and (f) $\Omega=2.6$ rad/s. Focusing occurred at $\Omega_{foc}=2.25$ rad/s. The contrast has been improved by subtracting successive video frames, as explained in the text. For clarity, lenses L1 and L2 (see Fig. 1) are not shown in the schematic insets.

Both in the normal liquid and in the superfluid state, down to our minimum temperature $T/T_c\simeq0.75$, focusing occurred [see Fig. 2(d)] at the same angular velocity, $\Omega_{foc}=2.25\pm0.10$ rad/s. This means that the superfluid surface had the same parabolic shape as the surface of the normal liquid at this Ω, i.e., that the equilibrium number of vortices was present in the illuminated region of the superfluid. At $T/T_c=0.75$, where $\rho_n/\rho=0.73$ [7], Eq. (2) predicts for the vortex-free state 1.17 times higher Ω_{foc}.

In certain rotating vessels it has been possible to prepare a vortex-free state of ^{3}He-B or a configuration with a vortex cluster in the center of the cell [8]. We investigated these possibilities for each of our types of measurements. For reasons that probably have to do with the availability of suitable nucleation centers at the walls and with the large radius of OC, a state with the equilibrium number of vortices was always observed in the illuminated area.

In these measurements, the rotation axis of the cryostat had to be tilted by about 0.1° to reflect the light beam from the liquid surface onto the camera. The beam

moved across the CCD sensor during a short fraction of each revolution. This, and the fountain effect to be described later, enabled us to increase the contrast of the interference pattern by subtracting two successive video frames, 20 ms apart, from each other by a computer. For this reason, focused light is seen as a black and a white spot in Fig. 2(d). Circular interference fringes at $\Omega=0$ in Fig. 2(a) were formed because the shape of the reference surface WW was slightly curved, which helped observation of the interference pattern. When the cryostat was rotated and the liquid surface became curved, the distance between the fringes decreased [Figs. 2(b) and 2(c)].

Light reflected from the reference surface WW provided a means to study the meniscus at an arbitrary Ω. For these experiments the rotation axis of the cryostat was adjusted to be parallel with gravity, so that the precession described earlier was eliminated. The rotating liquid with its parabolic surface forms a concave lens, which expands the returning beam as shown in Fig. 3(a). To determine the magnitude of this divergence, the displacement **D** of several inhomogeneities from their positions at $\Omega=0$ was measured using an image processing computer program. The magnitude of **D** is directly proportional to the slope of the liquid surface at each particular location. For a classical liquid or for a superfluid with equilibrium density of vortices, $dz(r)/dr=\Omega^2 r/g$ according to Eq. (1).

The displacement, whose magnitude $|\mathbf{D}|$ is proportional to Ω^2, is shown for several features in a typical video picture by the arrows in Fig. 3(b), both when the sample was superfluid at $T/T_c<0.85$ and when it was normal liquid at $T>T_c$. The common expansion center, corresponding to the rotation axis, is seen, from the convergence of the arrows, to be in the lower left corner of the frame, outside the luminous region; the arrows for the feature 4 do not, however, seem to originate from the same point as the others, probably because the edge of the illuminated area is so near that it affects the determination of the apparent motion of that feature. In Fig. 3(c), dz/dr, at the point of the circular feature labeled by 1 in Fig. 3(b), has been presented as a function of Ω^2, in both the normal and superfluid states. The slope was determined from $|\mathbf{D}|$ for this feature. No significant differences between the normal liquid and the superfluid could be observed. A calibration of $|\mathbf{D}|$ against dz/dr was made by tilting the stationary cryostat to 0°–0.5°.

For a classical liquid, the slope of the surface would be the same as in Fig. 3(c) at a distance $r=4.4$ mm from the rotation axis, in rough agreement with Fig. 3(b) where the diameter of the luminous area corresponds to about 6 mm in the cell. The relative change in the distance between features 2 and 3 [see Fig. 3(b)], which cannot be caused by a mere tilt of the liquid surface but must be due to its curvature, is presented in Fig. 3(d), for both normal liquid and the superfluid. The magnitude of expansion is in reasonable agreement with that calculated

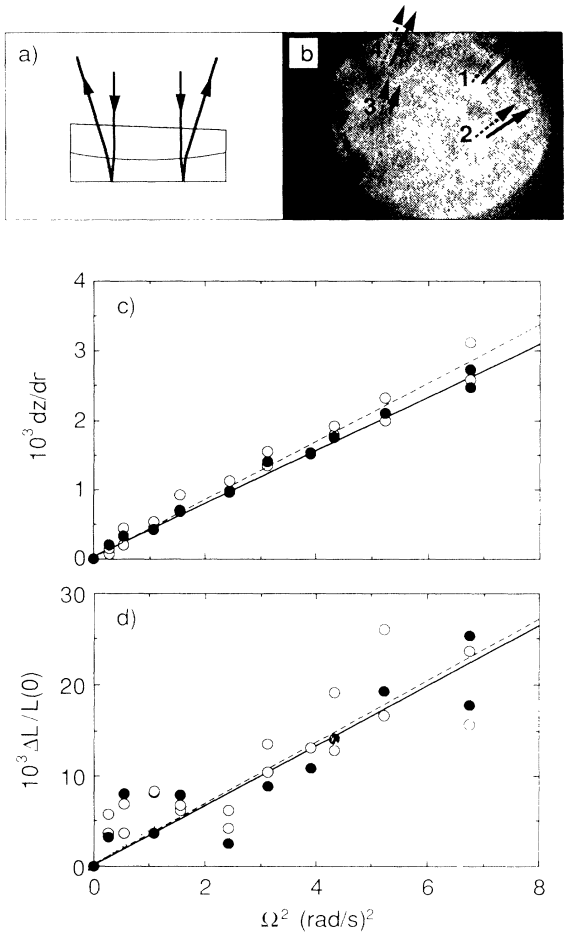

FIG. 3. (a) Principle of expansion of the light beam by the parabolic liquid surface. (b) Displacement **D** of several inhomogeneities, shown by the arrows, scaled by 100 (rad/s)$^2/\Omega^2$, in the superfluid state at $T/T_c<0.85$ (dotted arrows) and in the normal liquid at $T>T_c$ (solid arrows). (c) Slope of the ^{3}He surface, determined from the magnitude of **D**, at the point of feature 1 [see (b)] for $T/T_c<0.85$ (open circles; least squares fit to the data points by dashed line) and for $T/T_c\gg 1$ (solid circles; solid line) as a function of Ω^2. (d) The relative change $\Delta L/L(0)$ in the distance between features 2 and 3 at $T/T_c<0.85$ and at $T/T_c\gg 1$; $\Delta L=L(\Omega)-L(0)$, where $L(\Omega)$ is the separation when the angular velocity of the cryostat is Ω. The dotted line is calculated for a classical fluid using our calibration of $|\mathbf{D}|$ vs dz/dr (see text); the other symbols are as in (c).

on the basis of the calibration of $|\mathbf{D}|$ against dz/dr for a classical liquid with a meniscus of the form (1). Within the rather large scatter of our data, no difference between the measurements made in the superfluid state and in normal liquid could be observed; in a vortex-free superfluid, expansion would be scaled by $\rho_n/\rho<0.85$ at $T/T_c<0.85$.

Optical interference under continuous illumination let us observe, in an elegant way, the fountain effect on a thin layer of superfluid ^{3}He-*B*. A special superleak was

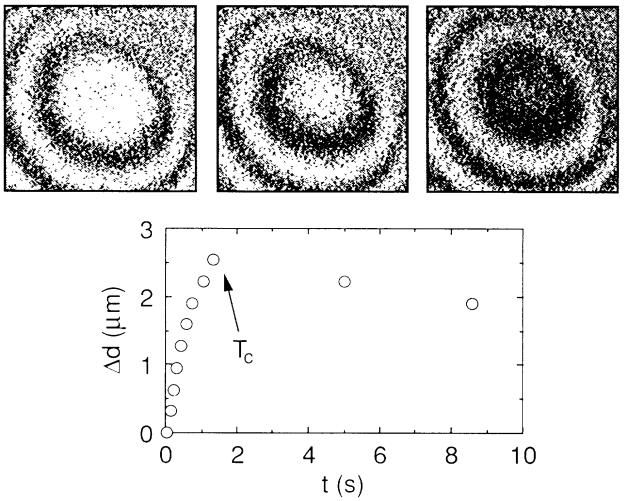

FIG. 4. Upper part: Illustration of the shrinking interference rings in the superfluid state due to the fountain effect. From left to right, the three pictures were taken at 20-ms intervals, and their contrast was increased by subtracting successive frames as in Fig. 2. Lower part: Increase of the sample thickness Δd as a function of time after illumination at the maximum attainable light power was started when $T < T_c$. Each datum corresponds to a change by one-half of the optical wavelength. The thickness of the ^{3}He layer at start was $d = 0.5$ mm.

not necessary, because the viscous normal component of the thin sample was immobile on the bottom of the experimental chamber. In the superfluid state, the interference rings moved under continuous illumination towards their center (see Fig. 4), where the curved reference surface WW (see Fig. 1) has its maximum; this means that the amount of liquid within the beam area increased, owing to the fountain effect, as presented in the lower part of the illustration. The thickness could increase as much as 10 μm during a few seconds. The superfluid component thus rushed into the illuminated region, trying to reduce the temperature differences in the sample. After the liquid had warmed into the normal state, the surface started to flatten. The thickening of the superfluid sample during illumination cannot be explained by thermal expansion [9] which, in our chamber, ought to increase the liquid level only by less than 0.03 μm when the superfluid warms from $T = 0.75T_c$ to T_c.

In conclusion, we have shown that it is possible to make visual observations, by taking advantage of modern fiber optics, at temperatures below 1 mK. The surface of rotating ^{3}He-B, both above and below T_c, had the curvature expected of a classical liquid; this indicates that, in our experimental cell, the equilibrium number of vortices was always observed in the superfluid state. The fountain effect in ^{3}He-B was seen as a thickening of the liquid layer in the illuminated region. We are presently improving our optical technique to detect the dimples produced by individual vortices [10], which was not possible in the present setup.

We thank G. Frossati and V. P. Mineev for useful discussions and Olga Andreeva for assistance during the construction of the optical apparatus. We are also grateful to M. Kaivola, T. Kajava, P. Kiiveri, S. Tammela, J. Turunen, and A. Vasara for help in problems concerning optics. Scholarships from the Emil Aaltonen Foundation (A.J.M.) and the Vilho, Yrjö, and Kalle Väisälä Foundation (H.A.) are acknowledged with thanks.

[a]Present address: Department of Physics, University of Jyväskylä, P.O. Box 35, 40351 Jyväskylä, Finland.

[1] D. V. Osborne, Proc. Phys. Soc. London Sect. A **63**, 909 (1950).

[2] P. L. Marston and W. M. Fairbank, in *Quantum Fluids and Solids,* edited by S. B. Trickey, E. D. Adams, and J. W. Dufty (Plenum, New York, 1977), p. 411; P. L. Marston, Ph.D. thesis, Stanford University, 1976.

[3] R. P. Feynman, in *Progress in Low Temperature Physics,* edited by C. J. Gorter (North-Holland, Amsterdam, 1955), Vol. 1, p. 17.

[4] G. A. Williams and R. E. Packard, Phys. Rev. Lett. **33**, 280 (1974).

[5] P. E. Wolf, F. Gallet, S. Balibar, and E. Rolley, J. Phys. (Paris) **46**, 1987 (1985); K.-P. Müller and D. Haarer, Phys. Rev. Lett. **66**, 2344 (1991).

[6] P. Hakonen, O. V. Lounasmaa, and J. Simola, Physica (Amsterdam) **160B**, 1 (1989).

[7] J. M. Parpia, D. G. Wildes, J. Saunders, E. K. Zeise, J. D. Reppy, and R. C. Richardson, J. Low Temp. Phys. **61**, 337 (1985).

[8] Y. Kondo, J. S. Korhonen, Ü. Parts, M. Krusius, O. V. Lounasmaa, and A. D. Gongadze, Physica (Amsterdam) **178B**, 90 (1992).

[9] G. W. Swift and R. E. Packard, J. Low Temp. Phys. **43**, 517 (1981).

[10] K. C. Harvey and A. L. Fetter, J. Low Temp. Phys. **11**, 473 (1973).

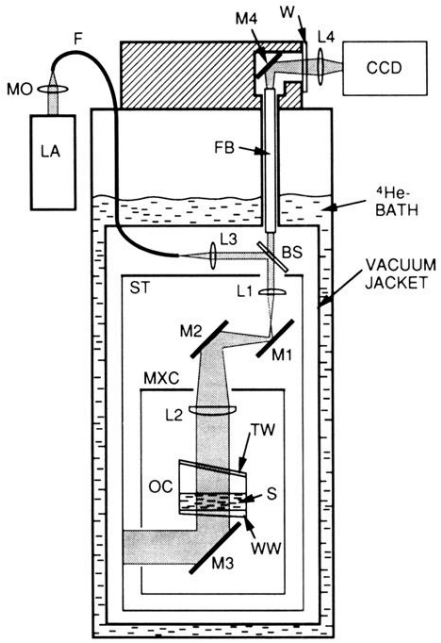

FIG. 1. Schematic illustration of the experimental setup (not to scale). Explanation of symbols: MO, microscope objective; M1, . . . , M4, aluminum coated mirrors; W, window. For other abbreviations, see text.

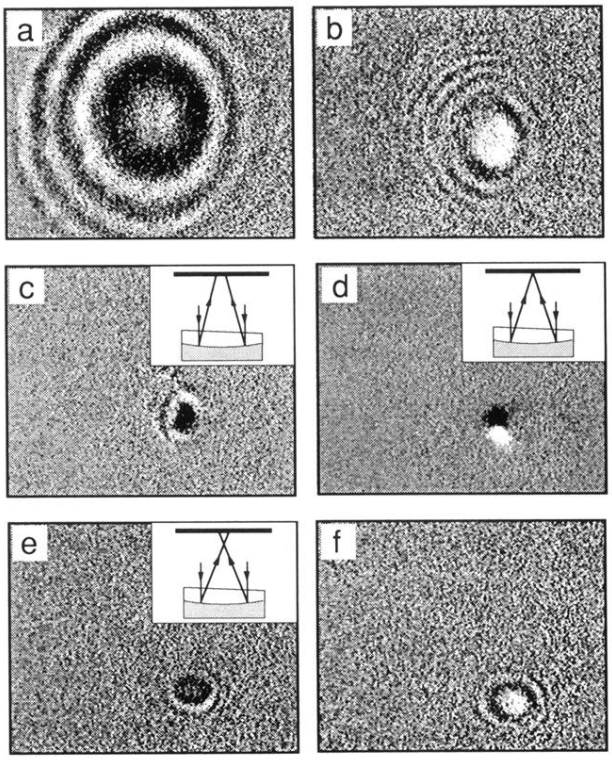

FIG. 2. Interference patterns produced by light reflected from the bottom window WW of the sample cell OC (see Fig. 1) and from the superfluid surface at $T/T_c \simeq 0.75$. (a) $\Omega = 0$, (b) $\Omega = 1.6$ rad/s, (c) $\Omega = 2.0$ rad/s, (d) $\Omega = 2.25$ rad/s, (e) $\Omega = 2.5$ rad/s, and (f) $\Omega = 2.6$ rad/s. Focusing occurred at $\Omega_{foc} = 2.25$ rad/s. The contrast has been improved by subtracting successive video frames, as explained in the text. For clarity, lenses L1 and L2 (see Fig. 1) are not shown in the schematic insets.

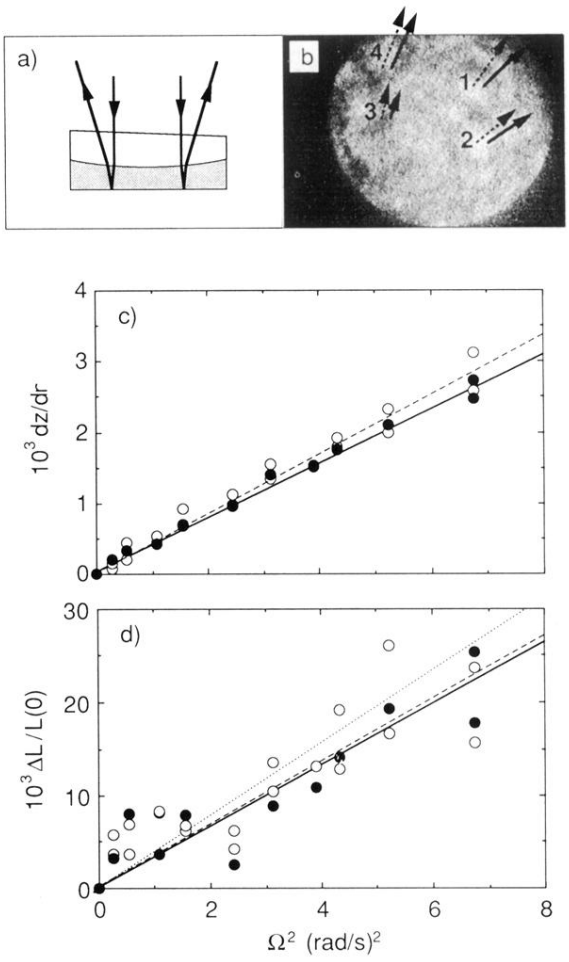

FIG. 3. (a) Principle of expansion of the light beam by the parabolic liquid surface. (b) Displacement **D** of several inhomogeneities, shown by the arrows, scaled by 100 $(\text{rad/s})^2/\Omega^2$, in the superfluid state at $T/T_c < 0.85$ (dotted arrows) and in the normal liquid at $T > T_c$ (solid arrows). (c) Slope of the ^{3}He surface, determined from the magnitude of **D**, at the point of feature 1 [see (b)] for $T/T_c < 0.85$ (open circles; least squares fit to the data points by dashed line) and for $T/T_c \gg 1$ (solid circles; solid line) as a function of Ω^2. (d) The relative change $\Delta L/L(0)$ in the distance between features 2 and 3 at $T/T_c < 0.85$ and at $T/T_c \gg 1$; $\Delta L = L(\Omega) - L(0)$, where $L(\Omega)$ is the separation when the angular velocity of the cryostat is Ω. The dotted line is calculated for a classical fluid using our calibration of $|\mathbf{D}|$ vs dz/dr (see text); the other symbols are as in (c).

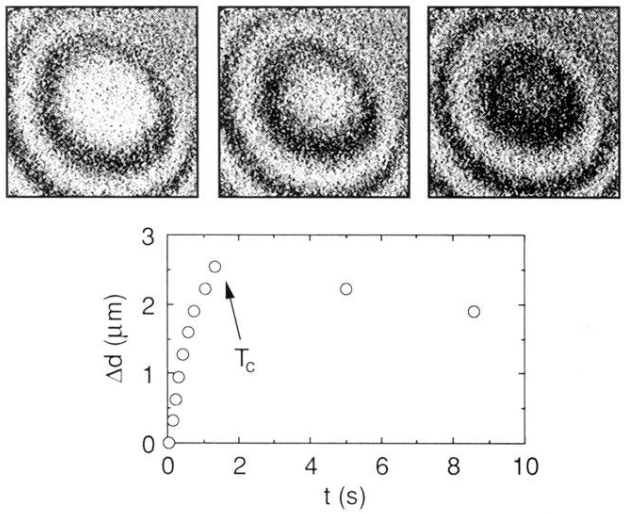

FIG. 4. Upper part: Illustration of the shrinking interference rings in the superfluid state due to the fountain effect. From left to right, the three pictures were taken at 20-ms intervals, and their contrast was increased by subtracting successive frames as in Fig. 2. Lower part: Increase of the sample thickness Δd as a function of time after illumination at the maximum attainable light power was started when $T < T_c$. Each datum corresponds to a change by one-half of the optical wavelength. The thickness of the ^{3}He layer at start was $d = 0.5$ mm.